Next Energy 9 (2025) 100467

Contents lists available at ScienceDirect

Next Energy

journal homepage: www.sciencedirect.com/journal/next-energy

Research article

Simulation-guided investigation of the effect of 2D perovskites on performances of 2D/3D mixed dimensional perovskite solar cells

Walagedara G.A. Pabasara[a,b], Udugama K.D.M. Akmal[a], Galhenage A. Sewvandi[a,*]

[a] Department of Materials Science and Engineering, Faculty of Engineering, University of Moratuwa, Katubedda, Moratuwa 10400, Sri Lanka
[b] Department of Engineering Technology, Faculty of Technology, University of Ruhuna, Karagoda, Uyangoda, Kamburupitiya 81100, Sri Lanka

ARTICLE INFO

Keywords:
Perovskite solar cells
2D perovskite
Stability
Efficiency
Solar cell capacitance simulator (SCAPS)

ABSTRACT

2D/3D mixed-dimensional Perovskite Solar Cells (PSCs) have attracted a great interest of scientists due to their balanced efficiency and stability. A detailed parametric investigation on 2D/3D mixed-dimensional PSCs is crucial to provide clear guidance for high-performance device fabrication. In this simulation-based study, 2D/3D mixed-dimensional PSCs were modeled using solar cell capacitance simulator (SCAPS)-1D software. The simulations were done by varying the thicknesses, defect densities, and recombination rates of the 2D and 3D layers, as well as interface defect densities and the series and shunt resistances of the device. The modeled device architecture was FTO/TiO_2/$MAPbI_3$/$BDAMA_3Pb_4I_{13}$/Cu_2O/Au, with $BDAMA_3Pb_4I_{13}$ and $MAPbI_3$ serving as the 2D and 3D perovskite layers, respectively. The results reveal that the defect density and the recombination rate of the 2D perovskite layer minimally influence performance compared to the 3D perovskite layer. Furthermore, the 3D/ETL interface is the dominant interface in charge transportation, while the HTL/2D interface has a negligible effect. The optimum performance occurred at a 2D layer thickness of 30 nm, 3D layer thickness of 1500 nm, with a 3D layer defect density of 1×10^{12} cm^{-3} and a recombination rate of 1×10^{-13} cm^3/s. The performance, PCE, V_{oc}, J_{sc} and FF, at aforementioned optimized conditions are 26.56%, 1.19 V, 25.09 mA/cm^2, and 89.13%, respectively. This study delivers valuable insights into experimental designs of 2D/3D mixed dimensional PSCs.

1. Introduction

Perovskite solar cells (PSC) are gaining tremendous attention all over the world due to their enhanced efficiency, cost effectiveness, and potential scalability [1]. Within a few decades, the power conversion efficiency (PCE) of PSCs has increased from 4% to over 26%, approaching the efficiency levels of conventional Si solar cells [2,3]. This significant growth of the PSC can be attributed to the continuous research efforts and application of advanced technologies leading to improved fundamental properties such as enhanced carrier mobility, better light absorption, and reduced recombination losses [4]. Even though PSCs have achieved over 26% PCE, they are less commercial due to their instability when exposed to moisture, elevated temperatures, and ultraviolet (UV) radiation. The performance of the devices is greatly reduced under these conditions, making them less abundant in commercial markets [5]. Numerous solutions have been proposed to overcome the stability issues faced by PSCs, including device encapsulations, compositional engineering, processing of additives, and charge transport layer modifications [6]. Experimental investigations have proved that 2D perovskite materials exhibit enhanced long-term stability compared to 3D counterparts [7,8]. 2D perovskite materials are represented by $(RNH_3)_2(A)_{n-1}B_nX_{3n+1}$, where R is a large organic cation and A, B, X, n are a monovalent cation, a divalent metal cation, a halide anion, and the number of inorganic $[PbX_6]^{4-}$ octahedral layers, respectively. The organic cation functions as a spacer cation between the inorganic perovskite layers, creating a layered structure containing alternative organic and inorganic components. This layered configuration facilitates the separation of the inorganic layers, contributing to the development of a 2D structural framework. The enhanced stability of 2D perovskites compared to their 3D counterparts can be explained through several synergistic mechanisms. Hydrophobic bulky organic spacer layers serve as protective barriers against moisture and oxygen, limiting the chemical degradation. Further, reduced dimensionality and organic interlayers suppress ion migration, reducing electrically driven instability [9,10]. Large organic cations also passivate defects and grain boundaries, reducing trap states and associated thermal or photochemical degradation. Further, larger exciton binding energy and stronger quantum confinement effects of 2D perovskite materials help

* Corresponding author.
E-mail address: galhenagea@uom.lk (G.A. Sewvandi).

https://doi.org/10.1016/j.nxener.2025.100467
Received 28 May 2025; Received in revised form 20 September 2025; Accepted 25 September 2025

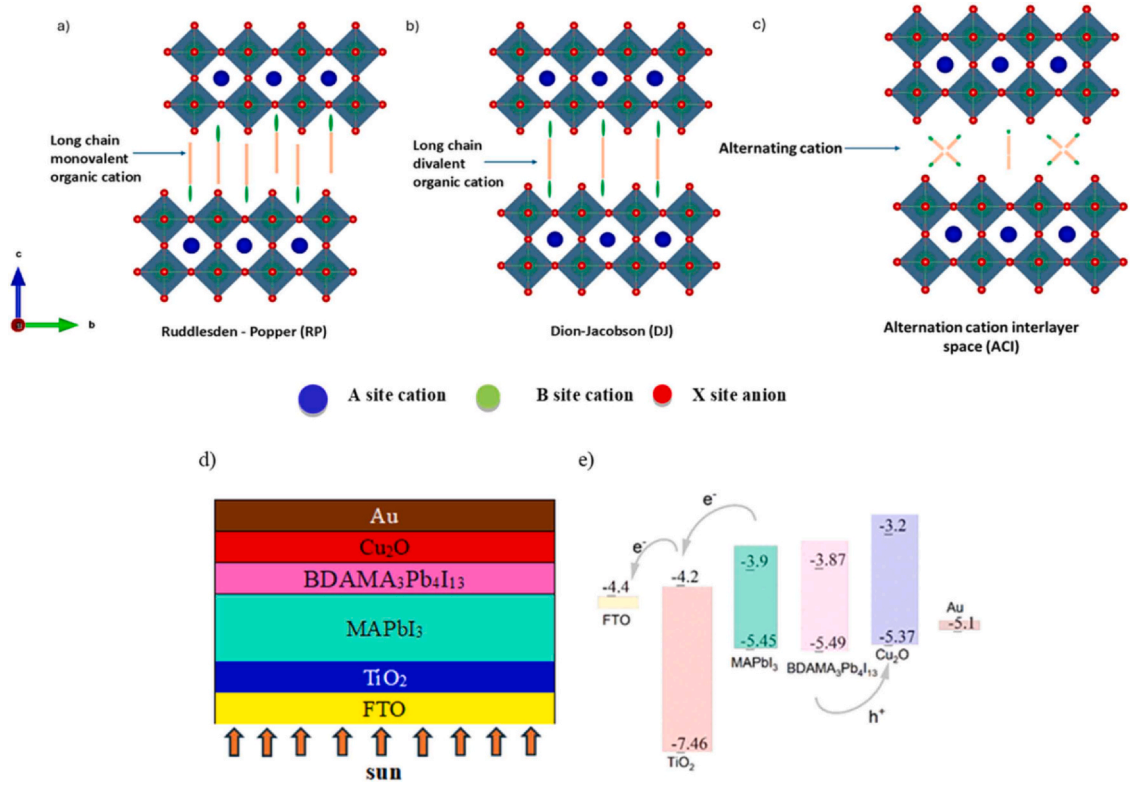

Fig. 1. Main categories of 2D perovskites; (a) Ruddlesden–Popper (RP), (b) Dion–Jacobson (DJ), and (c) Alternation cation in the interlayer space perovskites (ACI), (d) Device architecture, (e) Corresponding energy band diagram of the proposed device.

to reduce thermal fluctuations and nonradiative recombination rates, strengthening the intrinsic stability [11,12].

2D perovskites can be broadly classified into 3 main categories based on the structure of large organic cations, as shown in Fig. 1: Ruddlesden–Popper (RP), Dion–Jacobson (DJ), and Alternation Cation in the Interlayer space (ACI) perovskites [13]. RP phase contains monoamine-based larger organic cations such as butyl ammonium [$CH_3(CH_2)_3$–NH_3^+], phenyl ethyl ammonium [$C_6H_5(CH_2)_2$–NH_3^+]. DJ perovskites comprise diamine cations such as pentamethylenediamine [H_3N^+–$(CH_2)_5$–NH_3^+] and hexamethylenediamine [H_3N^+–$(CH_2)_6$–NH_3^+]. ACI phase perovskites are relatively uncommon and feature guanidinium [$C(NH_2)_3^+$] spacer cation, alternating with a smaller monovalent cation (often methylammonium (MA^+)) in the interlayer space [13,14].

Among these categories, DJ perovskites have exhibited greater stability compared to the RP perovskites [8,15]. This can be preliminarily attributed to the absence of weak Van der Waals interactions and shorter interlayer distances. Furthermore, they are intrinsically stable because of the hydrogen bonding of spacer cations to the organic layers on both sides [13]. Moreover, DJ perovskites exhibit better charge transportation properties relative to RP perovskites due to the reduced quantum confinement of charge carriers, which results from shorter interlayer distances. The reduced interlayer spaces allow more efficient charge carrier mobility, improving the overall performance of the device [13]. A comparative study between DJ and RP-based PSCs has reported a 34% enhanced efficiency for DJ-based PSCs compared to RP-based PSCs [15]. Furthermore, DJ-based PSCs showed outstanding stability than RP-based PSCs, maintaining over 95% PCE after being subjected to rigorous conditions, including ambient air with 40%–70% relative humidity (RH), heating at 85 °C, and prolonged continuous light soaking [16].

Achieving both stability and efficiency concurrently is the major challenge faced by 3D and 2D perovskites individually. To address this, 2D perovskite materials, proven to be stable, are incorporated into 3D perovskite materials to boost the overall stability of the structure [6–9,14,15,17]. The resultant solar cells are recognized as 2D/3D mixed dimensional PSCs. However, the stability of the PSCs is yet to be significantly improved to achieve the stability protocols established by the International Summit on Organic Photovoltaic Stability (ISOS) for commercialization [17]. Despite the proven stability of the 2D perovskite materials, many of them remain unexplored for their ability to boost the stability of the 3D PSCs. Notably, the selection of the appropriate spacer group in the 2D perovskites plays a crucial role in determining the stability and performance of the mixed dimensional system [13–16].

1.4-butanediamine (BDA) spacer molecule-based DJ perovskite has been reported to have excellent stability under different environmental conditions [8,17,18]. BDA is a diamine with a 4-carbon alkyl chain linking 2 amino groups, H_2N-$(CH_2)_4$-NH_2, facilitating optimum structural flexibility and rigidity. The straight chain configuration promotes stronger hydrogen bonding between the layers, reinforcing the structural integrity and thereby improving the resistance to environmental degradation. The reduced interlayer distances between layers minimize the insulating barrier, promote better charge transportation and reduce the defect-induced recombination, leading to higher photovoltaic performances [8]. Despite these advantages, the feasibility of integration of BDA-based DJ perovskite material with 3D perovskite has not been systematically explored.

Therefore, this study focuses on the numerical simulation of novel 2D/3D mixed dimensional PSC by incorporating BDA-based DJ perovskites as a capping layer to the 3D-$CH_3NH_3PbI_3$ ($MAPbI_3$). A detailed parametric investigation on 2D/3D mixed-dimensional perovskite solar cells was performed, focusing on defect densities, recombination dynamics, and interface sensitivities, areas that are often underexplored in existing literature. This analysis provides valuable guidance to experimental researchers for designing and fabricating 2D/3D mixed dimensional PSCs. The findings of the study set a foundation for future experimental validations and real-world applications, paving the way towards the commercialization of perovskite solar cells.

2. Design and simulation methodology

The device architecture of the proposed 2D/3D mixed dimensional PSC is shown in Fig. 1(d). In the proposed design, considering the stability of the inorganic materials over organic materials, TiO_2 was selected as the electron transport layer (ETL), while Cu_2O was chosen as the hole transport layer(HTL). In the given cell architecture, $MAPbI_3$ acts as the 3D perovskite light absorbing layer, and $BDAMA_3Pb_4I_{13}$ is the 2D capping layer. Fluorine-doped tin dioxide (FTO) and Gold (Au) were placed as the front and the back electrode contacts, respectively. Therefore, the general architecture of the proposed cell is FTO/TiO_2/$MAPbI_3$/$BDAMA_3Pb_4I_{13}$/Cu_2O/Au.

As shown in Fig. 1(e), the valence band of Cu_2O is well aligned with that of the valence band of perovskite layers, facilitating efficient transport of photo-generated holes into the back contact Au electrode. Moreover, the conduction band of Cu_2O demonstrates a large offset from the conduction bands of the perovskite absorber layers, thereby effectively blocking the electron transport in that direction. Although the typical Cu_2O formation process requires high-temperature annealing, the reactive magnetron sputtering technique can be used to form Cu_2O film on highly sensitive underlying perovskite layers [20]. Furthermore, the conduction band of TiO_2 is well-aligned with that of $MAPbI_3$ and $BDAMA_3Pb_4I_{13}$ layers, enabling efficient extraction of electrons towards the FTO. This favorable band alignment facilitates efficient and effective charge separation and transportation, contributing to improved device performance.

SCAPS 1D (Solar Cell Capacitance Simulator) software was employed to simulate the proposed PSC. This software can be effectively used to examine the factors that govern the performance of the PSCs. It is instrumental in the identification of feasible and effective materials, configurations, and conditions to enhance the performance of the PSCs. The software uses Poisson's equation (Eq. 1), the electron continuity equation (Eq. 2), and the hole continuity equation (Eq. 3) to model the behavior of the solar cell [21].

$$\frac{d}{dx}\left(-\varepsilon(x)\frac{d\varphi}{dx}\right) = q\left[p(x) - n(x) + N_d^+(x) - N_a^-(x)\right] \tag{1}$$

$$\frac{\partial j_n}{\partial x} = q\left(R_n - G + \frac{\partial n}{\partial t}\right) \tag{2}$$

$$\frac{\partial j_p}{\partial x} = q\left(R_p - G + \frac{\partial p}{\partial t}\right) \tag{3}$$

where,

ε = permittivity, φ = electrostatic potential, q = electron charge, p = total hole density, N_d^+ = ionized donor-like doping concentration. N_a^- = ionized acceptor-like doping concentration, n = total electron density, j_n and j_p = electron and hole current densities, G = generation rate per unit volume, R_n and R_p = net recombination rates for electron and hole per unit volume.

The proposed cell configuration was drawn in the software, and simulation was performed using the drift-diffusion model at 300 K temperature upon one sun illumination (AM1.5 G, 1000 mW/cm^2). In this study, the SCAPS-1D simulations are performed, assuming static ion positions, so that the impact of ion migration and respective hysteresis phenomena are not reflected. The physical parameters used for SCAPS 1D simulations are shown in Table 1.

3. Results and discussion

3.1. Effect of thickness of perovskite layers on device performances

In this section, device performance dependence on both 2D and 3D perovskite layer thicknesses was investigated to determine the optimum thickness values for enhanced performance. The absorber layer thickness is paramount as it is a crucial factor in determining the amount of absorbed solar radiation. To study the impact of the thickness, the 2D perovskite layer thickness initially varied from 10 to 2000 nm, keeping the 3D perovskite layer thickness fixed at 500 nm. Fig. 2 indicates the behavior of photovoltaic parameters with the 2D perovskite layer thickness. Then, the 3D perovskite layer thickness varied from 10 to 2000 nm, keeping the 2D perovskite layer thickness at the optimum thickness value. It can be observed that at 30 nm of 2D perovskite layer and 1500 nm of 3D perovskite layer, the device yields the maximum PCE. When further increasing the thickness of 3D perovskite, PCE starts to decline slightly. Open circuit voltage (V_{oc}) and fill factor (FF) demonstrate a declining trend with thickness. However, short circuit current (J_{sc}) shows a sharp rise until 1000 nm thickness, and after that, the rate of increment diminishes.

This behavior can be attributed to light absorption, charge carrier generation and transport dynamics [34]. Generally, relatively thin perovskite layers absorb a small portion of longer wavelengths, resulting in fewer electron and hole pair generations. When the thickness improves, the absorption in long wavelengths increases, leading to more carrier pair generation, contributing to the observed rise in the J_{sc}. Further enhancing the thickness beyond a threshold thickness value, it may absorb a larger fraction of the longer wavelength and generate more carrier pairs, but the generated carriers have to travel longer distances to reach the respective electrodes, which increases carrier recombination, reducing the number of charge carriers available for current generation. This phenomenon leads to a reduction in the PCE after a critical thickness value, as shown in Fig. 2(a). In addition to that, the internal electric field within a device, which is affected by the built-in potential, is a driving force for the separation and collection of charge carriers. Enhanced thickness can affect this field, potentially decreasing its strength, which adversely affects the effective separation and transportation of charge carriers. This field modulation contributes to degrading performance by decreasing V_{oc} and FF. Moreover, when increasing thickness, series resistance starts to rise, reducing the voltage output of the device. Due to these 2 reasons, V_{oc} and FF are decreasing with the thickness as per Fig. 2(b) and (d) [19,34].

The contribution of the 2D layer in light absorption is limited compared to the 3D perovskite layer due to a relatively higher bandgap. Therefore, when increasing the thickness beyond 30 nm of the 2D perovskite layer, PCE decreases gradually as thicker layers impede charge transportation and enhance the recombination losses [27].

The modest increase in J_{sc} is mainly due to its minor role in light absorption and the dominance of the 3D layer in light absorption. The sharp decline of V_{oc} with increasing 2D perovskite layer thickness can be attributed to increased recombination and potential barriers, driven by the material's anisotropic charge transport and high exciton binding energy, which limit out-of-plane carrier mobility and promote trap-assisted recombination [21]. FF declines gradually because a thicker 2D layer increases series resistance and impedes charge transportation [35].

The 2D perovskite layer significantly affects V_{oc} and FF, reflecting limited charge extraction and increased recombination losses. In contrast, the 3D perovskite layer mainly governs PCE and J_{sc}, owing to its greater light-harvesting capabilities and efficient carrier transport, leading to higher photocurrent generation and overall device performance.

3.2. Effect of defect densities of the absorber layers on the performances

Perovskite materials often consist of abundant intrinsic defects, including antisites, vacancies, interstitials, impurities, Schottky and Frankel defects, as well as dangling bonds at the surface and the grain boundaries [22,35]. The perovskite film fabrication is mainly done using solution-based processes, which may add mid-gap states into the band structure. These gap states result in increased carrier recombination, reducing the carrier diffusion length and the charge

Table 1
Physical parameters used in SCAPS 1D simulation

Parameters	FTO	ETL (TiO_2)	HTL (Cu_2O)	$BDAMA_3Pb_4I_{13}$	$CH_3NH_3PbI_3$
	[22–24]	[1,15,22,25,26]	[15,27–29]	[30–32]	[1,15,25,33]
Layer thickness (nm)	500	100	30	10–2000	10–2000
Bandgap (eV)	3.5	3.26	2.20	1.62	1.55
Electron Affinity (eV)	4	4.2	3.40	3.85	3.9
Dielectric permittivity (relative)	9	38	7.11	16	3.2
Effective density of states of the conduction band C_B ($1/cm^3$)	2.2E + 18	2.2E + 17	2.5E + 17	6.88E + 18	2.8E + 20
Effective density of states of the valence band V_B ($1/cm^3$)	1.8E + 19	1.8E + 18	3.0E + 20	1.32E + 19	3.9E + 20
Electron thermal velocity (cm/s)	1.0E + 7	1.0E + 7	1.0E + 7	1.0E + 7	1.0E + 7
Hole thermal velocity (cm/s)	1.0E + 7	1.0E + 7	1.0E + 7	1.0E + 7	1.0E + 7
Electron mobility (cm^2/Vs)	20	2.0E + 4	200	2	11.8
Hole mobility (cm^2/Vs)	10	1.0E + 3	8600	2	11.8
Shallow uniform donor density N_D ($1/cm^3$)	2.0E + 19	6.0E + 19	0	0	1.0E + 9
Shallow uniform acceptor density N_A ($1/cm^3$)	1.0E + 15	0	1.0E + 18	0	1.0E + 9
Radiative recombination coefficient (cm^3/s)		1.0E−13	1.0E−13	1.0E−5–1.0E−10	1.0E−5–1.0E−10
Capture cross-section electrons (cm^2)		1.0E−15	1.0E−15	1.0E−15	1.0E−15
Capture cross-section holes (cm^2)		1.0E−15	1.0E−15	1.0E−15	1.0E−15
Reference for defect energy level E_t		0.1	0.1	0.1	0.1
Energy level with respect to the reference (eV)		0.6	0.6	0.6	0.6
Defect density	1.0E + 10	1.0E + 12	1.0E + 12	1.0E + 10–1.0E + 16	1.0E + 10–1.0E + 16

FTO = fluorine-doped tin dioxide; SCAPS = solar cell capacitance simulator; ETL= electron transport layer; HTL= hole transport layer

carrier lifetime. These defects are called deep and shallow level defects and typically range from 1×10^{10} cm^{-3} to 1×10^{11} cm^{-3}, and 1×10^{14} cm^{-3} to 1×10^{16} cm^{-3}, respectively [27]. Controlling the level of defect densities is essential to fabricating efficient and stable PSCs. As the majority of defects occur at the fabrication stage, they can be controlled by regulating the annealing temperature and thin film deposition process [36]. In this study, the effect of the defect densities of 2D and 3D perovskite layers was comprehensively investigated, varying the defect densities in the range of 1×10^{10} to 1×10^{16} cm^{-3} while keeping the thickness of the film at previously identified optimum values. Importantly, the current study assumes a uniform distribution of defects across the device layers. However, in real 2D/3D perovskite systems, spatial variations in defect density can affect device performance and stability [37]. The behavior of the photovoltaic parameters with defect densities is illustrated in Fig. 3.

In the 3D perovskite layer, the photovoltaic parameters are unaffected by defect densities up to a certain critical value. Beyond this threshold defect density, all parameters start to decline gradually. The

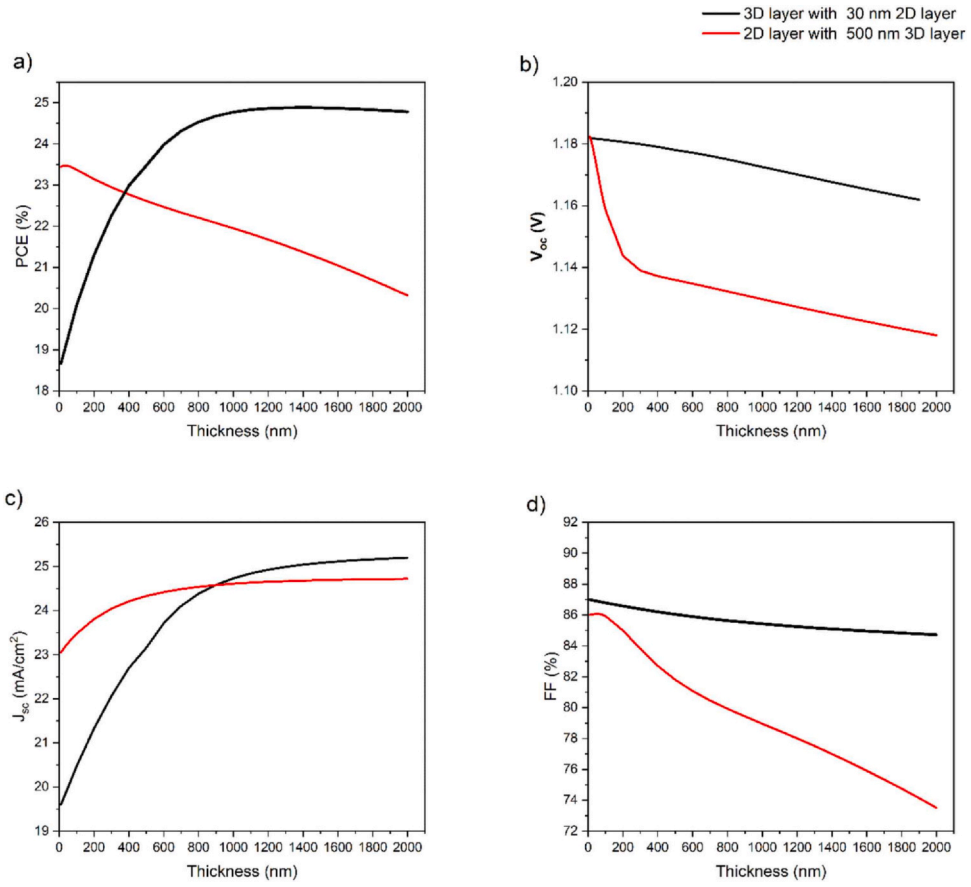

Fig. 2. Impact of 2D and 3D perovskite layer thickness on performances of 2D/3D mixed dimensional PSC; (a) PCE, (b) V_{oc}, (c) J_{sc}, and (d) FF. PCE = power conversion efficiency; V_{oc} = open circuit voltage; J_{sc} = short circuit current; FF = fill factor; PSCs = perovskite solar cells.

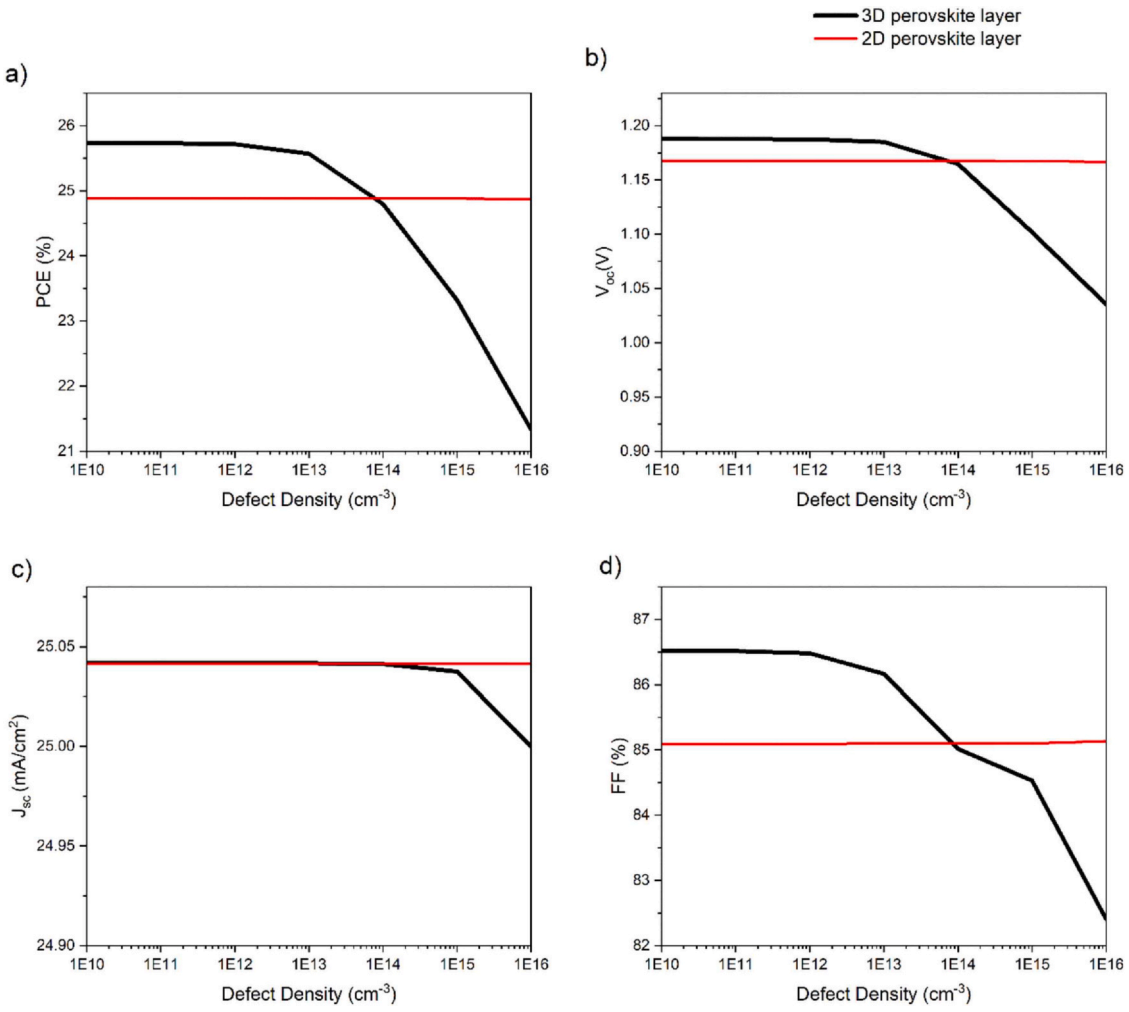

Fig. 3. Impact of 2D and 3D perovskite layer defect density on the performances of 2D/3D mixed dimensional PSC; (a) PCE, (b) V_{oc}, (c) J_{sc}, and (d) FF. PCE = power conversion efficiency; V_{oc} = open circuit voltage; J_{sc} = short circuit current; FF = fill factor; PSCs = perovskite solar cells.

critical defect density value of the 3D absorber layer is 1×10^{12} cm^{-3} with PCE of 25.72%, V_{oc} of 1.19 V, J_{sc} of 25.04 mA/cm^2, and FF of 86.48%. This decline can be preliminarily attributed to the increased recombination at higher defect densities. This phenomenon can be further described using the Shockley–Read–Hall (SRH) model. This model illustrates how defects of a semiconductor material can act as recombination centers for charge carrier pairs, thereby affecting the carrier dynamics and device performance, as mentioned in Eqs. (4) and (5) [15].

$$R_{SRH} = \frac{np - n_i^2}{\tau_p(n + n_i) + \tau_n(p + p_i)} \tag{4}$$

$$\tau_{n,p} = \frac{1}{\sigma v_{th,n,p} N_t} \tag{5}$$

Here, R_{SRH} represents the rate of the Shockley–Read–Hall recombination, n and p are the concentrations of electrons and holes, respectively. τ_p, τ_n are the lifetimes of the electron and hole. $\upsilon_{th,n,p}$ are the thermal velocities of electrons and holes, respectively. At relatively low defect density levels, the recombination rate (R_{SRH}) remains minimal, facilitating the majority of the photo-generated carriers to be effectively collected by the electrodes before recombination occurs [33]. As a result of that, up to a certain defect density threshold, the device performance remains unaffected. However, as the defect density level rises to moderate and higher values, trap states become prominent, and the performance starts to drop. As per Eq. (5), defect density (N_t) is inversely related to the lifetime of the electron and hole. Thus, defect density increases, and the nonradiative recombination is enhanced, diminishing the overall performance of the device [38].

The effect of defect densities of the 2D perovskite layer on device performance is displayed in Fig. 3. According to the simulation results, the performances are unaffected by the variations in defect density of the 2D perovskite layer. This may be due to the dominance of the thicker 3D perovskite layer (1500 nm) in light absorption. In this case, most generated charge carriers are collected from the 3D perovskite layer, rendering the defects in the 2D perovskite layer insignificant in the performance of the PSC. Furthermore, the effect of the 2D perovskite layer carrier mobility on device performance was examined. The results reveal that variations in the 2D layer's carrier mobility have a negligible impact on the key photovoltaic metrics, owing to the relatively thin nature of the 2D layer. (Fig. S1 in Supporting Information).

3.3. Effect of defect density at 2D/3D interface on device performances

The interfacial defects that serve as charge recombination centers in PSCs arise from the structural mismatch between particular materials or contamination of environmental impurities. In this study, the effect of 3 interfaces in the device, the 2D/HTL interface, the 2D/3D interface, and the 3D/ETL interface, was comprehensively investigated to optimize the performance.

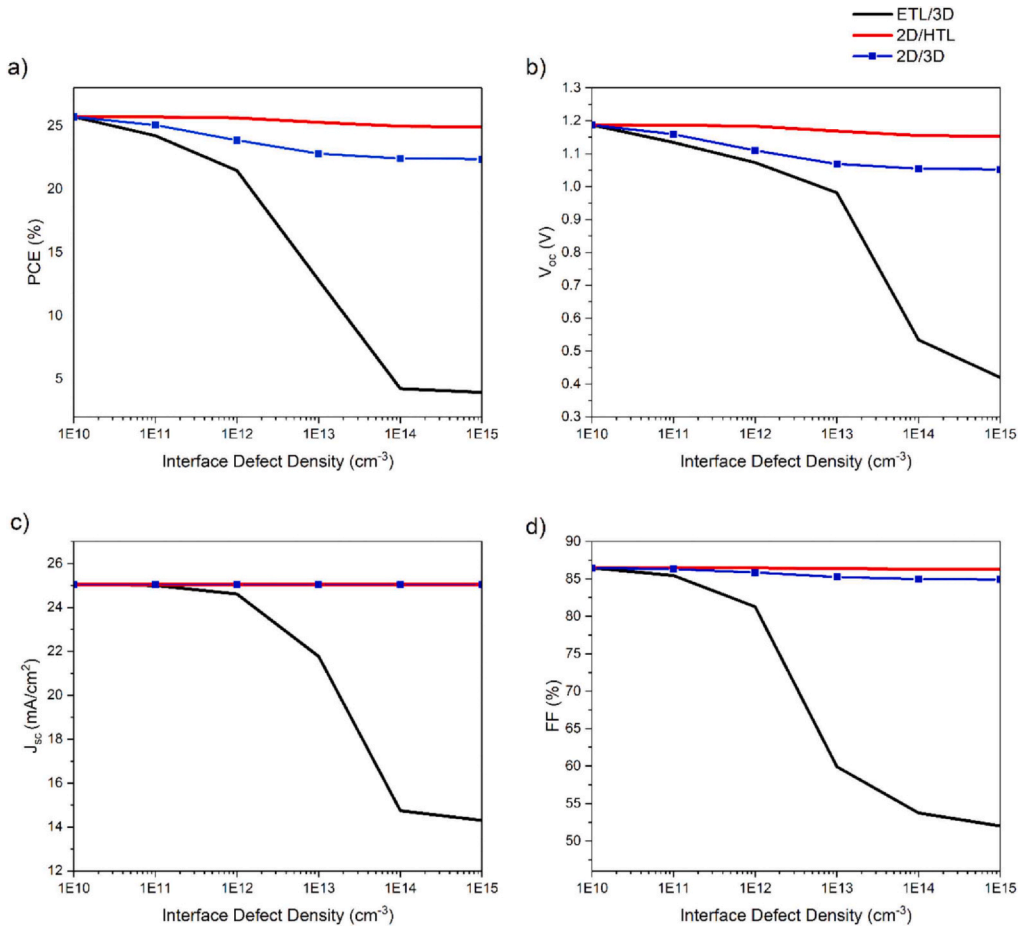

Fig. 4. Impact of defect density at HTL/2D,3D/ETL, 2D/3D interfaces on the performances of 2D/3D mixed dimensional PSC; (a) PCE, (b) V_{oc}, (c) J_{sc}, and (d) FF. PCE = power conversion efficiency; V_{oc} = open circuit voltage; J_{sc} = short circuit current; FF = fill factor; PSCs = perovskite solar cells.

The interface between 2D and 3D perovskite layers is prominent in determining the performance of 2D/3D mixed dimensional PSCs [27]. The smooth interfaces with minimal defects are favorable for high-efficiency PSCs. In third-generation solar cell technology, solution-based fabrication methods are critical in regulating these defects and improving the performance and stability of the devices [22]. In this study, to comprehensively investigate the impact interface at the 2D/3D perovskite layers, the defect density varied between 1×10^{10} cm^{-3} to 1×10^{15} cm^{-3}. Fig. 4 demonstrates how the photovoltaic parameters behave according to the defect density variation. There is a notable decline in device performance when increasing the interface defect density, and maximum values are given at 1×10^{10} cm^{-3}. When increasing interface defect density from 1×10^{10} cm^{-3} to 1×10^{15} cm^{-3}, PCE declines from 25.72% to 22.37% while V_{oc} decreases from 1.19 to 1.05 V. Furthermore, FF declines from 86.48% to 84.92%. In contrast, J_{sc} remains relatively stable, exhibiting minimal change as depicted in Fig. 4(c).

3.4. Effect of defect density at HTL/2D and 3D/ETL interfaces on device performance

The impact of HTL/2D and 3D/ETL interface defect densities on the device performance was investigated, altering the interface defect density over the range of 1×10^{10} cm^{-3} to 1×10^{15} cm^{-3}. All the photovoltaic parameters, PCE, V_{oc}, and FF, show a significant decline with increasing the defect density at the 3D/ETL interface as per Fig. 4. The PCE declines from 25.72 to 3.93% when increasing the defect density from 1×10^{10} cm^{-3} to 1×10^{15} cm^{-3}, and V_{oc} decreases from 1.19 to 0.42 V. Similarly, FF and J_{sc} also drop to 52.01% and 14.3 mA/cm^{-3}, respectively, at 1×10^{15} cm^{-3}. Increasing defect density at the 3D/ETL interface results in higher carrier recombination rates, leading substantial reduction in V_{oc} and J_{sc}, and, hence, a decreased FF. The combined effect of these factors causes a significant decline in PCE [39].

As shown in Fig. 4, unlike the effect of 3D/ETL interface defect density, all photovoltaic parameters show a negligible response to the defect density variations at the HTL/2D interface. At the ETL (TiO_2)/3D ($MAPbI_3$) interface, the negative conduction band offset (–0.3 eV) forms a cliff-like structure. This reduces the electron barrier, allowing efficient electron extraction. However, it leads to electron accumulation at the ETL/3D interface. The deep defect states (10^{14}–10^{16} cm^{-3}) at this interface serve as strong Shockley–Read–Hall (SRH) recombination centers, where injected electrons recombine with holes from the perovskite, which enhances the charge recombination velocity [40]. A higher recombination velocity directly reduces the carrier collection efficiency, since majority of photogenerated electrons are lost at the interface instead of being extracted into the ETL. Consequently, the effective carrier lifetime decreases, the dark saturation current rises and the device suffer a significant loss in V_{oc}, accompanied by reduced fill factor and power conversion efficiency.

Therefore, the ETL/3D interface is highly sensitive to defect density. In contrast, the HTL (Cu_2O)/2D ($BDAMA_3Pb_4I_{13}$) interface demonstrates favorable band alignment with an uphill offset for holes (0.12 eV) that aids hole extraction, and a significant electron barrier (0.67 eV) that blocks electron flow. This minimizes the interfacial electron density and SRH recombination at the HTL/2D interface, and ensures efficient hole transfer to HTL without degrading the performance [41].

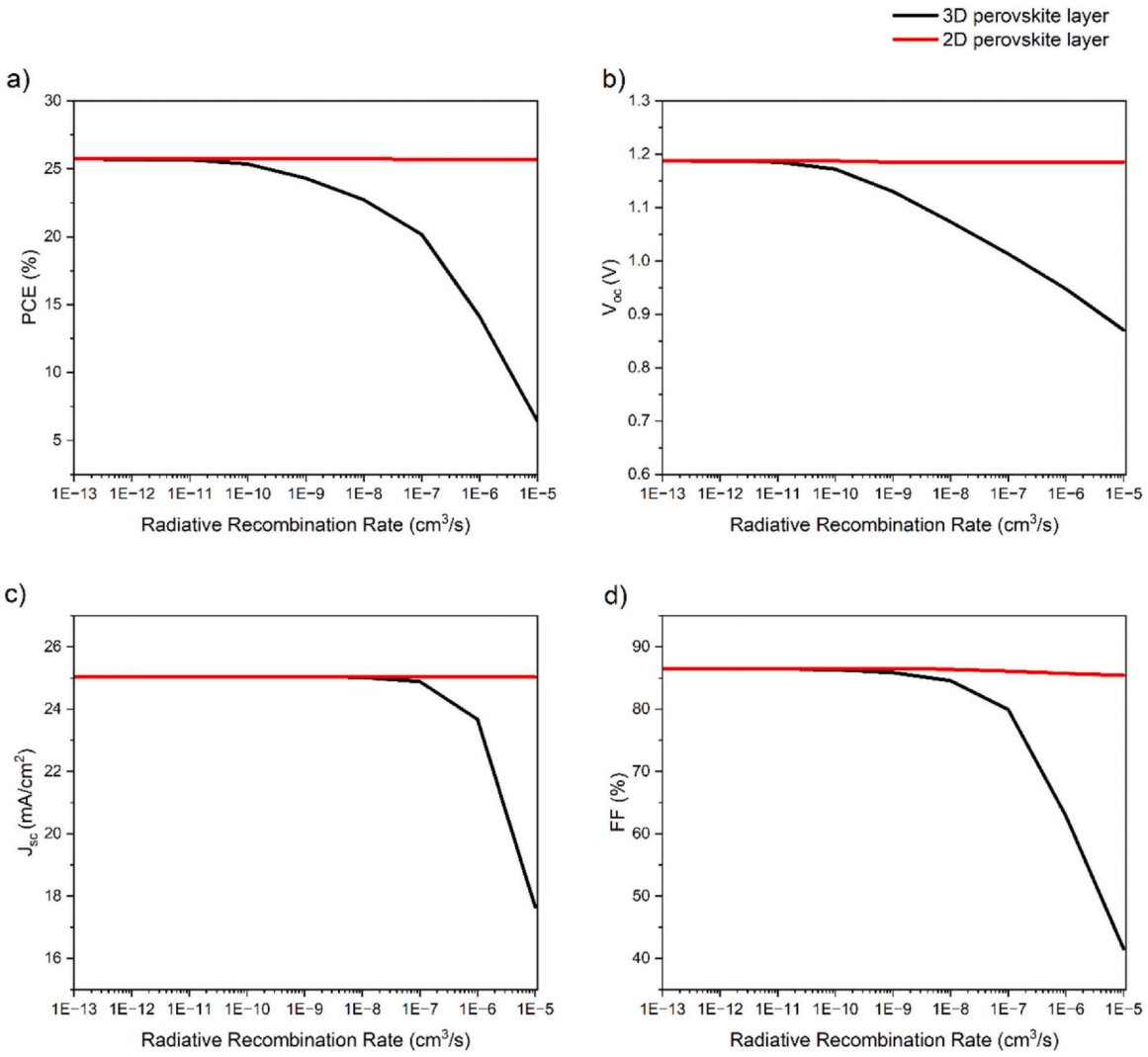

Fig. 5. Impact of band-to-band radiative recombination rate of 2D and 3D perovskite layers on the performances of 2D/3D mixed dimensional PSC; (a) PCE, (b) V_{oc}, (c) J_{sc}, and (d) FF. PCE = power conversion efficiency; V_{oc} = open circuit voltage; J_{sc} = short circuit current; FF = fill factor; PSCs = perovskite solar cells.

3.5. Effect of band-to-band radiative recombination rate on device performance

In the perovskite materials, there are 3 key recombination mechanisms, namely, the band-to-band (Radiative), Shockley–Read–Hall (SRH), and Auger recombination. In Augur recombination, energy is absorbed by free charge carriers [42]. The Augur recombination mechanism is significant only at higher penetration levels. In SRH recombination, which is affected by defect states and densities. It is mainly related to the processing and deposition of materials and device fabrication [43]. The band-to-band recombination, also known as radiative recombination, can be defined as the process in which an electron in the conduction band recombines with a hole in the valence band, emitting a photon. In perovskite materials, when a photon is absorbed, an electron is injected into the conduction band, creating a metastable state. However, electrons can relax back to the valence band, where they recombine with holes, leading to a stable state. This overall process is called band-to-band radiative recombination. The rate of radiative recombination in the perovskite layer is affected by the carrier density of states [44].

In this section, the dependence of the photovoltaic parameters on band-to-band radiative recombination rate is comprehensively analyzed, ranging from 1×10^{-13} cm^3/s to 1×10^{-5} cm^3/s. The PCE decreases from 25.72% to 6.39% when the recombination rate of the 3D perovskite layer rises within the selected range, Fig. 5(a). The V_{oc} declines linearly from 1.19 to 0.87 V when increasing the recombination rate of the 3D perovskite layer, as per Fig. 5(b). The J_{sc} remains relatively stable until 1×10^{-9} cm^3/s and then starts to decline gradually, as per Fig. 5(c). The FF factor also exhibits a downward trend when increasing the recombination rate, as shown in Fig. 5(d). When the radiative recombination rate increases, the concentration of electrons present in the conduction band declines, which in turn reduces the internal electric field. Subsequently, this decline in the electric field leads to lower V_{oc}, J_{sc}, and PCE, diminishing the performance of the PSC.

When considering the radiative recombination rate in the 2D perovskite layer, the impact is insignificant as per Fig. 5. All photovoltaic parameters show negligible response when changing the recombination rate of the 2D layer. As the 2D perovskite layer acts as a capping layer in the solar cell and its less contribution to the light absorption and carrier generation, the impact has become negligible [45,46].

3.6. Effect of series resistance (R_s) and shunt resistance (R_{sh}) on device performance

R_s and R_{sh} possess a substantial impact on device performance. R_s originated from electrical resistance associated with the front and back contacts, and interfaces, as well as electrical dissipation within the ETL,

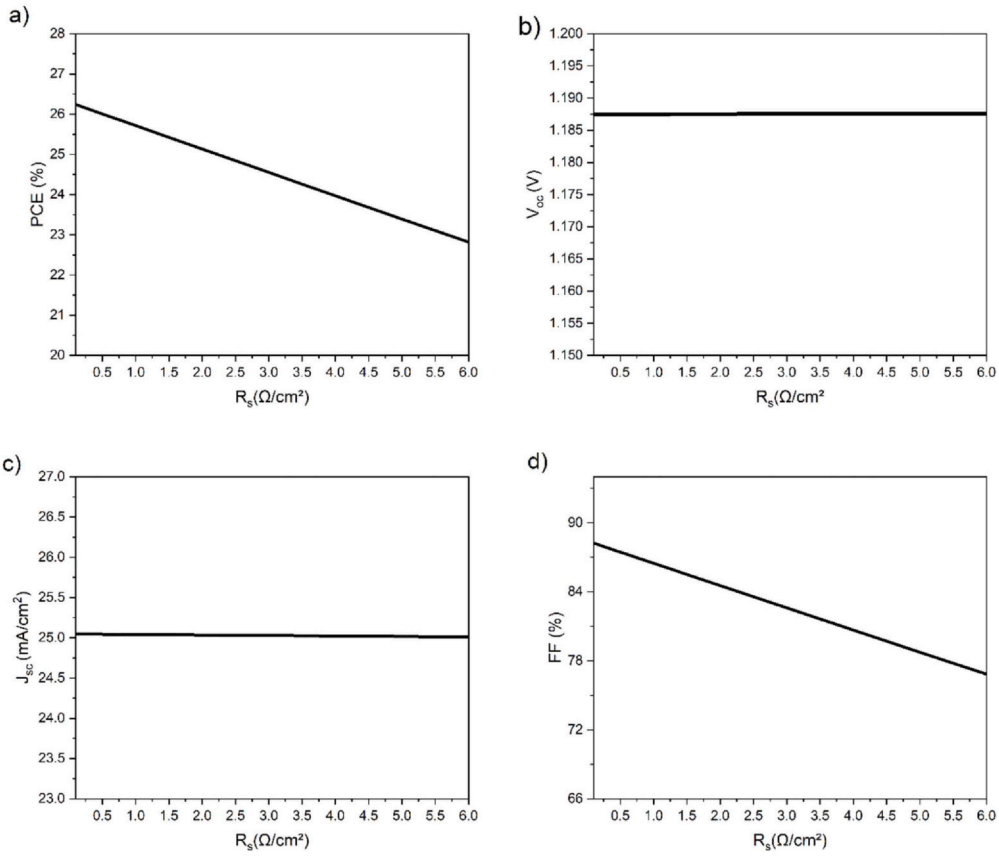

Fig. 6. Impact of R_s on the performance of 2D/3D mixed dimensional PSC; (a) PCE, (b) V_{oc}, (c) J_{sc} and (d) FF. PCE = power conversion efficiency; V_{oc} = open circuit voltage; J_{sc} = short circuit current; FF = fill factor; PSCs = perovskite solar cells.

HTL, and absorber layers [47]. R_{sh} represents several alternative charge recombination paths that are highly affected by device design, including edge effects. A low R_{sh} leads to photovoltage loss, and it can reduce the collected photocurrent. Meanwhile, R_s preliminary affects the FF and PCE. It is essential to maintain a low R_s and a high R_{sh} to achieve a high efficiency level in PSCs [22].

As shown in Fig. 6, when increasing the R_s from 0.1 to 6 Ω/cm^2, PCE drops from 26.30 to 22.82% while FF decreases to 76.83% from the initial value of 88.43%. V_{oc} remains almost constant at 1.19 V without being affected by R_s variation. J_{sc} exhibits an insignificant decline of 25.05–25.01 mA/cm^2 when R_s is varied in the given range. These findings are well aligned with previous simulation reports [22,43,44].

$$P_{loss} = J_{sc}^2 R_S \tag{6}$$

As depicted in Eq. (6), power loss and R_s have a positive relationship [48,49]. Therefore, power loss can be minimized by reducing the R_s. The resistance in the interfaces and electrodes can be effectively reduced by employing a suitable fabrication process and implementing interface modifiers. Furthermore, selecting appropriate materials or dopants in ETL and HTL can greatly reduce the bulk resistance of the device, improving the performance [50].

To rigorously examine the influence of R_{sh} on the device performance, the R_{sh} values were systematically varied over a range from 10^2 to 10^6 Ω/cm^2. As displayed in Fig. 7, a significant rise in PCE is observed from 15.13 to 26.56% when the R_{sh} is increased from 10^2 to 10^6 Ω/cm^2. FF also shows a remarkable increment from 51.57 to 89.13% with the increasing R_{sh}. V_{oc} and J_{sc} remain relatively stable without significant change.

In PSCs, improper designs and fabrication errors often substantially reduce the R_{sh}, which can lead to higher leakage currents and lower efficiency levels. Moreover, when back contact materials with low work functions are used, J_{sc} decreases, which subsequently diminishes the PCE of the PSC.

Ensuring optimum design and applying back-contact materials with appropriate work functions are necessary for maximizing R_{sh} and sustaining high device performance [22].

3.7. Effect of operating temperature on device performance

The operating temperature of the device directly influences the power output of the solar cell. In the practical scenario, solar panels are installed outdoors, and they often operate at over 300 K. Studies have reported that elevated temperatures can increase stress and strain within the device, leading to increased interfacial defects and disorders. Consequently, this adversely affects the interlayer connectivity between layers, compromising device stability and efficiency [51]. Higher temperature level has an impact on the bandgap, carrier concentrations, carrier mobilities, and density of states [22].

In the current study, the dependence of the performance on operating temperature was evaluated by changing the temperature within the range of 300–380 K. As per Fig. 8, all photovoltaic parameters decrease when the temperature increases. The highest performances, PCE, V_{oc}, J_{sc}, and FF are 26.56%, 1.19 V, 25.09 mA/cm^2, and 89.13%, respectively, can be observed at 300 K. The increasing temperature declines the PCE due to the temperature-induced carrier transportation effect in the PSC [22]. Increasing temperature reduces the carrier diffusion lengths, promoting carrier recombination and thereby reducing the PCE. Furthermore, series resistance rises with temperature enhancement, thereby declining the FF. Additionally, at elevated temperatures, more interfacial defects are generated, leading to higher series resistance and reduced diffusion length, which decreases the V_{oc} [51].

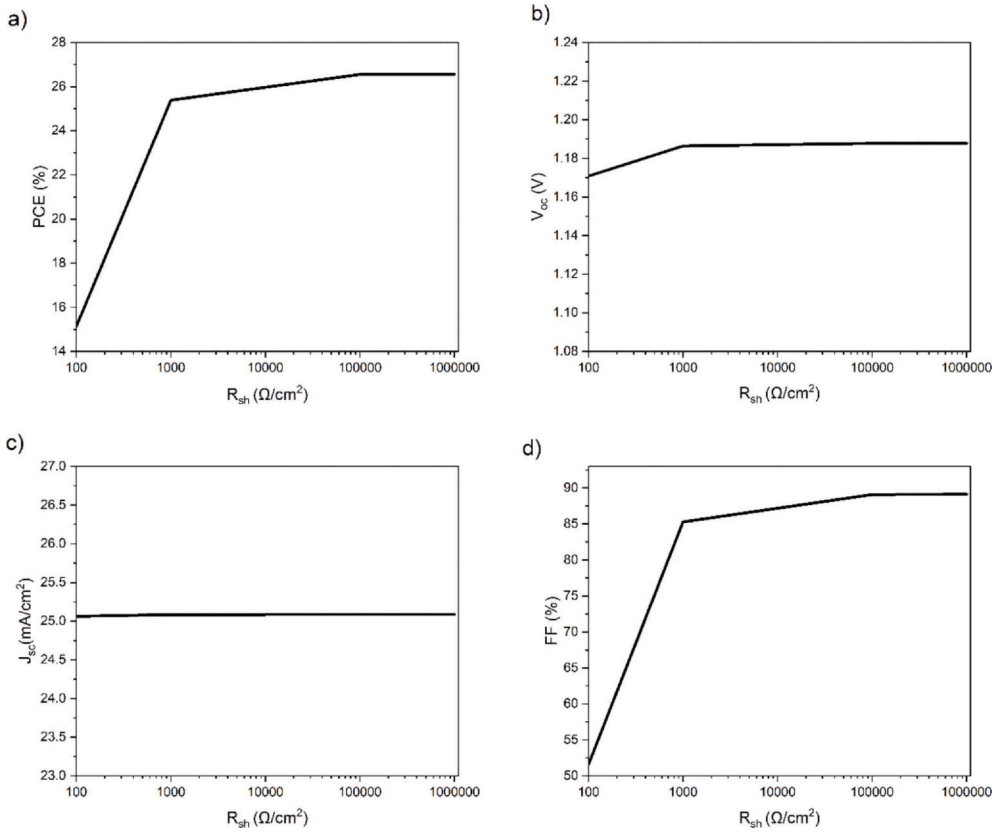

Fig. 7. Impact of R_{sh} on the performances of 2D/3D mixed dimensional PSC; (a) PCE, (b) V_{oc}, (c) J_{sc}, and (d) FF. PCE = power conversion efficiency; V_{oc} = open circuit voltage; J_{sc} = short circuit current; FF = fill factor; PSCs = perovskite solar cells.

3.8. Photovoltaic characteristics of the optimized device configuration

The selected solar cell configuration of FTO/TiO_2/$MAPbI_3$/$BDAMA_3Pb_4I_{13}$/Cu_2O/Au was optimized by varying the absorber layer thicknesses, defect densities, recombination rate, series, and shunt resistances. The comparison of I-V and QE (quantum efficiency) characteristics of the optimized 2D/3D mixed dimensional PSC and the 3D PSC without the 2D perovskite capping layer is illustrated in Fig. 9. Furthermore, the photovoltaic parameters of 2 device configurations are depicted in Table 2. The 2 curves show a slight difference, specifically, the J_{sc} of the 2D/3D mixed dimensional PSC is slightly higher than the 3D PSC, while V_{oc} is slightly lower. The 2D perovskite capping layer has increased the PCE by 8.32% in 2D/3D mixed dimensional solar cells.

According to Fig. 9(b), QE behavior was observed as a function of wavelength. The 2D/3D mixed-dimensional PSC maintains a higher QE across the visible spectrum (380–750 nm) compared to the 3D perovskite based PSC, indicating more efficient charge collection and light harvesting. These results verify the optical quality of the DJ-phase 2D capping layer and its role in improving performance without introducing optical losses.

This study highlights the photovoltaic performance benefits of incorporating a DJ phase 2D perovskite material ($BDAMA_3Pb_4I_{13}$) in a 2D/3D mixed-dimensional structure. However, due to limitations of the SCAPS-1D simulation platform, which assumes static ions and does not support environmental degradation modeling, it is essential to note that the stability of 2D/3D structures attributed to the 2D layer remains hypothetical within the scope of this simulation study. Therefore, any stability-related claims due to the 2D layer are mainly supported by well-documented literature findings rather than by the present simulation study.

The enhanced stability of 2D perovskites is primarily attributed to their layered architecture, in which large organic spacer cations form hydrophobic barriers that effectively protect the perovskite structure from moisture and oxygen penetration. DJ 2D perovskites incorporate divalent organic spacer cations that form stronger hydrogen bonds with adjacent inorganic layers on both sides, resulting in shorter interlayer distances, enhanced structural rigidity, reduced ion migration, and reduced susceptibility to environmental degradation. This compact structure also enhances dielectric screening and mitigates quantum confinement of charge carriers, contributing to enhanced charge transport [8,13].

When considering the already reported experimental studies, Time Resolved Photoluminescence (TRPL) measurements have shown a longer carrier lifetime in 2D/3D perovskites than pure 3D perovskites. An increased Fermi-level splitting has been identified with the introduction of the 2D capping layer on 3D perovskites [46]. These effects are attributed to reduced defect density and suppressed nonradiative recombination, resulting from the effective surface passivation by the 2D layer [46]. Moreover, 2D/3D stacking configurations have experimentally demonstrated enhanced long-term environmental stability [8,18], retaining over 90% original PCE under prolonged ambient air exposure and continuous illumination without encapsulation [45]. However, detailed stability-focused simulations, such as modeling the effects of humidity or temperature cycling, and accelerated aging tests for experimental validation, can be recommended for future work.

The results of the study have been compared with the other existing simulation studies, as mentioned in Table 3. The performance of the proposed device, FTO/TiO_2/$MAPbI_3$/$BDAMA_3Pb_4I_{13}$/Cu_2O/Au, with a PCE of 26.56%, is supported by comparing simulation studies. Compared to RP-phase $BA_2MA_3Pb_4I_{13}$ in an inverted configuration, our device demonstrates a clear performance gain due to the enhanced charge extraction and transport facilitated by the DJ-phase $BDAMA_3Pb_4I_{13}$. While the $PeDAMA_4Pb_5I_6$-based device delivers a slightly lower PCE, the close agreement in key photovoltaic parameters validates the reliability of our simulations.

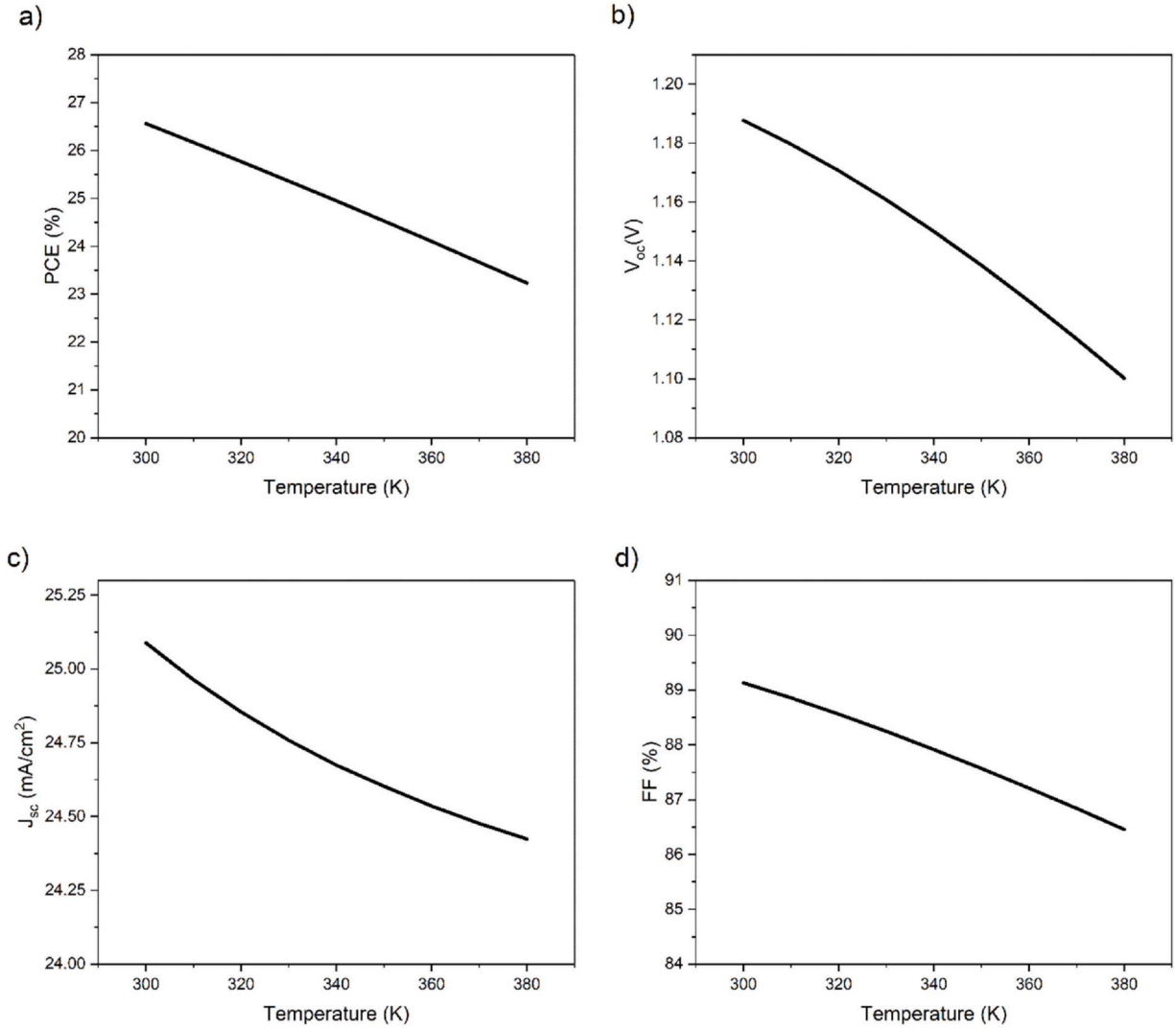

Fig. 8. Impact of operating temperature on the performances of 2D/3D mixed dimensional PSC; (a) PCE, (b) V_{oc}, (c) J_{sc}, and (d) FF. PCE = power conversion efficiency; V_{oc} = open circuit voltage; J_{sc} = short circuit current; FF = fill factor; PSCs = perovskite solar cells.

When benchmarking the simulated results against the experimental findings, some simulated results exceed the experimentally recorded values, especially the PCE, due to idealized conditions used in the modeling, such as uniform doping, defect densities, and layer morphology. However, actual perovskite films contain impurities and structural non-uniformities which are not fully considered during the

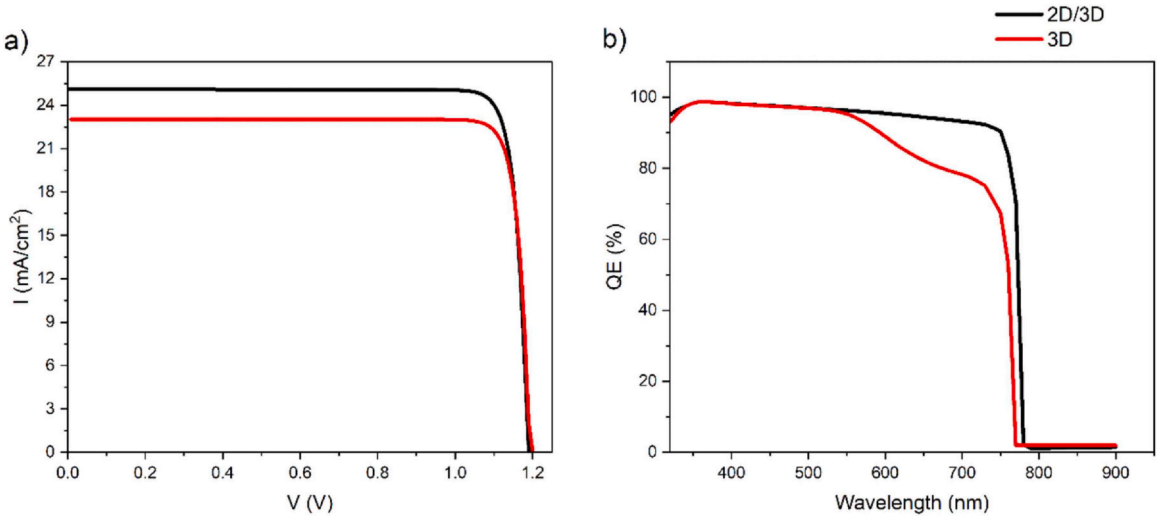

Fig. 9. (a) I-V and (b) QE characteristics comparison optimized device. QE = quantum efficiency.

Table 2
Comparison of photovoltaic parameters of the 3D PSC and the 2D/3D mixed dimensional PSC

Device	PCE (%)	V_{oc} (V)	J_{sc} (mA/cm^2)	FF (%)
FTO/TiO_2/$MAPbI_3$/Cu_2O/Au	24.52	1.19	23.00	89.37
FTO/TiO_2/$MAPbI_3$/$BDAMA_3Pb_4I_{13}$/Cu_2O/Au	26.56	1.19	25.09	89.13

FTO = fluorine-doped tin dioxide; PCE = power conversion efficiency; V_{oc} = open circuit voltage; J_{sc} = short circuit current; FF = fill factor

Table 3
Comparison of the findings with existing simulation and experimental results

Device architecture	PCE (%)	V_{oc} (V)	J_{sc} (mA/cm^2)	FF (%)
FTO/TiO_2/$MAPbI_3$/$BDAMA_3Pb_4I_{13}$/Cu_2O/Au (this study)	26.56	1.19	25.09	89.13
ITO/Cu_2O/$BA_2MA_3Pb_4I_{13}$/$MAPbI_3$/TiO_2/Al (simulated) [27]	18.46	0.98	24.77	77.44
FTO/TiO_2/$MAPbI_3$/$PeDAMA_4Pb_5I_{16}$/Spiro-OMeTAD (simulated) [15]	26.03	1.43	20.78	87.73
FTO/SnO_2/$FA_{0.85}MA_{0.10}Cs_{0.05}Pb(I_{0.9}Br_{0.1})_3$/BDAPbI$_4$/Spiro-OMeTAD (experimental) [45]	20.32	1.13	24.1	74.6
FTO/TiO_2//$Cs_{0.05}(FA_{0.83}MA_{0.17})_{0.95}Pb(I_{0.83}Br_{0.17})_3$/ PEA_2PbI_4/Spiro-OMeTAD (experimental) [46]	18.51	1.11	22.89	73.00

FTO = fluorine-doped tin dioxide; PCE = power conversion efficiency; V_{oc} = open circuit voltage; J_{sc} = short circuit current; FF = fill factor

SCAPS 1D simulation. Furthermore, simulations provide only simplified interfaces, neglecting the full complexity of recombination and carrier extraction at interfaces. Experimentally derived performance is also influenced by real-world factors such as light intensity, heat and moisture, which are not fully accounted for in SCAPS 1D simulations. Despite these disparities, consistent performance trends can be observed between simulation and experiment results, which reinforces the credibility of our simulation approach. Even though the current study is purely numerical, the proposed $BDAMA_3Pb_4I_{13}$ 2D perovskite composition has already been synthesized and utilized in operating PSCs, validating its practical viability and potential use as a capping layer in the 3D perovskites [52,53].

4. Conclusion

In this study, the 2D/3D mixed dimensional PSC with device architecture (FTO/TiO_2/$MAPbI_3$/ $BDAMA_3Pb_4I_{13}$/Cu_2O/Au) was numerically simulated and optimized using SCAPS 1D software, varying different parameters such as the thickness, the recombination rate, the defect density, and the temperature. The optimized device achieved a notable PCE of 26.56% with a V_{oc} of 1.19 V, J_{sc} of 25.09 mA/cm^2, and FF of 89.13%, highlighting the effectiveness of the 2D/3D mixed dimensional configuration. The results indicate that the 3D/ETL interface plays a major role in charge transport compared to the HTL/2D layer. Furthermore, the defect density and the recombination rate of the 2D perovskite layer have a limited effect on performance compared to the 3D layer. This study unveils the promising paths to design and fabricate 2D/3D mixed dimensional PSCs using DJ perovskite materials.

Funding sources

This research did not receive any specific grant from funding agencies in the public, commercial, or not-for-profit sectors.

CRediT authorship contribution statement

Walagedara G.A. Pabasara: Conceptualization, Methodology, Simulation and analysis, Writing – original draft, Review & editing. **Muditha D. Akmal:** Simulation. **Galhenage A. Sewvandi:** Supervision, Writing – review & editing.

Data availability statement

Data and other supportive findings will be available on reasonable request from the corresponding author.

Declaration of Competing Interest

The authors declare that they have no known competing financial interests or personal relationships that could have appeared to influence the work reported in this paper.

Acknowledgments

The authors sincerely acknowledge Prof. Marc Burgelman and his team at the University of Gent, Belgium, for their invaluable effort in creating, maintaining and freely distributing the SCAPS-1D software, which was instrumental in performing the solar cell simulations in this research.

Appendix A. Supporting material

Supplementary data associated with this article can be found in the online version at doi:10.1016/j.nxener.2025.100467.

References

[1] M.K.A.A. Mohammed, et al., Harnessing the potential of Dion-Jacobson perovskite solar cells: insights from SCAPS simulation techniques, J. Alloy. Compd. 963 (March) (2023) 171246, https://doi.org/10.1016/j.jallcom.2023.171246.
[2] H. Min, et al., Perovskite solar cells with atomically coherent interlayers on SnO_2 electrodes, Nature 598 (7881) (2021) 444–450, https://doi.org/10.1038/s41586-021-03964-8.
[3] G.H. Kim, D.S. Kim, Development of perovskite solar cells with > 25% conversion efficiency, Joule 5 (5) (2021) 1033–1035, https://doi.org/10.1016/j.joule.2021.04.008.
[4] M.-H. Li, et al., Highly efficient 2D/3D hybrid perovskite solar cells via low-pressure vapor-assisted solution process, Adv. Mater. 30 (30) (2018) e1801401, https://doi.org/10.1002/adma.201801401.
[5] B.P. Kore, M. Jamshidi, J.M. Gardner, The impact of moisture on the stability and degradation of perovskites in solar cells, Mater. Adv. 5 (6) (2024) 2200–2217, https://doi.org/10.1039/d3ma00828b.
[6] S. Mazumdar, Y. Zhao, X. Zhang, Stability of perovskite solar cells: degradation mechanisms and remedies, Front. Electron 2 (August) (2021) 1–34, https://doi.org/10.3389/felec.2021.712785.
[7] E.B. Kim, M.S. Akhtar, H.S. Shin, S. Ameen, M.K. Nazeeruddin, A review on two-dimensional (2D) and 2D-3D multidimensional perovskite solar cells: perovskites structures, stability, and photovoltaic performances, J. Photochem. Photobiol. C Photochem. Rev. 48 (June 2020) (2021) 100405, https://doi.org/10.1016/j.jphotochemrev.2021.100405.
[8] T. Niu, et al., Reduced-dimensional perovskite enabled by organic diamine for efficient photovoltaics, J. Phys. Chem. Lett. 10 (10) (2019) 2349–2356, https://doi.org/10.1021/acs.jpclett.9b00750.
[9] K. Ma, J. Sun, L. Dou, Advances and challenges in molecular engineering of 2D/3D perovskite heterostructures, Chem. Commun. 60 (61) (2024) 7824–7842, https://doi.org/10.1039/d4cc02299h.
[10] J. Zhang et al., Environmental Science efficiency perovskite solar cells in ambient air using an automated device acceleration platform†, pp. 5490–5499, 2024, doi:10.1039/d4ee01432d.
[11] B. Li, et al., Fundamental understanding of stability for halide perovskite photovoltaics: the importance of interfaces, Chem 10 (1) (2024) 35–47, https://doi.org/10.1016/j.chempr.2023.09.002.

[12] Y. Zhao, et al., A bilayer conducting polymer structure for planar perovskite solar cells with over 1,400 hours operational stability at elevated temperatures, Nat. Energy 7 (2) (2022) 144–152, https://doi.org/10.1038/s41560-021-00953-z.
[13] T.L. Leung, I. Ahmad, A.A. Syed, A.M.C. Ng, J. Popović, A.B. Djurišić, Stability of 2D and quasi-2D perovskite materials and devices, Commun. Mater. 3 (1) (2022) 1–10, https://doi.org/10.1038/s43246-022-00285-9.
[14] S. Ahmad, X. Guo, Rapid development in two-dimensional layered perovskite materials and their application in solar cells, Chin. Chem. Lett. 29 (5) (2018) 657–663, https://doi.org/10.1016/j.cclet.2017.08.057.
[15] S. Chaurasia, et al., Highly efficient and stable Dion–Jacobson(DJ) 2D-3D perovskite solar cells with 26% conversion efficiency: a SCAPS-1D study, J. Phys. Chem. Solids 191 (January) (2024) 112038, https://doi.org/10.1016/j.jpcs.2024.112038.
[16] S. Ahmad, et al., Dion-Jacobson phase 2D layered perovskites for solar cells with ultrahigh stability, Joule 3 (3) (2019) 794–806, https://doi.org/10.1016/j.joule.2018.11.026.
[17] M.V. Khenkin, et al., Consensus statement for stability assessment and reporting for perovskite photovoltaics based on ISOS procedures, Nat. Energy 5 (1) (2020) 35–49, https://doi.org/10.1038/s41560-019-0529-5.
[18] Y. Zhang, et al., Roles of organic ligands in ambient stability of layered halide perovskites, ACS Appl. Mater. Interfaces 14 (29) (Jul. 2022) 33085–33093, https://doi.org/10.1021/acsami.2c05348.
[19] W. Zhou, D. Li, D. Zhang, H. Tang, H. Zhang, C. Liang, Electronic and optical absorption properties of organic-inorganic perovskites as influenced by different long-chain diamine molecules: first-principles calculations, RSC Adv. 9 (26) (2019) 14718–14726, https://doi.org/10.1039/c9ra03042e.
[20] B.A. Nejand, V. Ahmadi, S. Gharibzadeh, H.R. Shahverdi, Cuprous oxide as a potential low-cost hole-transport material for stable perovskite solar cells, ChemSusChem 9 (3) (Feb. 2016) 302–313, https://doi.org/10.1002/cssc.201501273.
[21] M. Burgelman, K. Decock, A. Niemegeers, J. Verschraegen, and S. Degrave, SCAPS manual, pp. 7–8, 2025.
[22] S.T. Jayawardane, et al., Simulation-based performance analysis of lead-free bismuth perovskite solar cells: a comparative study of $Cs_3Bi_2I_9$ and $(CH_3NH_3)_3Bi_2I_9$ -based perovskite solar cells, Adv. Theory Simul. 7 (7) (2024) 2400206, https://doi.org/10.1002/adts.202400206.
[23] S. Samaki, F. Tchangnwa Nya, G.M. Dzifack Kenfack, A. Laref, Materials and interfaces properties optimization for high-efficient and more stable RbGeI3 perovskite solar cells: optoelectrical modelling, Sci. Rep. 13 (1) (2023) 15517, https://doi.org/10.1038/s41598-023-42471-w.
[24] S. Das, et al., Electron transport layer material optimization for $Cs_2AgBiBr_6$ based solar cell using SCAPS, J. Nano Electron. Phys. 16 (1) (2024) 4–7, https://doi.org/10.21272/jnep.16(1).01014.
[25] M. Hasan, et al., Impact of absorber layer thickness and defect density on the performance of $MAPbI_3$ solar cells based on CuO_2 as hole transport material, Eng. Res. Express 5 (3) (2023) e06379, https://doi.org/10.1088/2631-8695/acfb5a.
[26] M.T. Islam, et al., Numerical simulation studies of $Cs_3Bi_2I_9$ perovskite solar device with optimal selection of electron and hole transport layers, Optik (Stuttg) 231 (2021) 166417, https://doi.org/10.1016/j.ijleo.2021.166417.
[27] J. Chakrabartty, M.A. Islam, S. Reza, Performance analysis of highly efficient 2D/3D bilayer inverted perovskite solar cells, Sol. Energy 230 (October) (2021) 195–207, https://doi.org/10.1016/j.solener.2021.10.007.
[28] P. Sawicka-Chudy, M. Sibiński, G. Wisz, E. Rybak-Wilusz, M. Cholewa, Numerical analysis and optimization of Cu_2O/TiO_2, CuO/TiO_2, heterojunction solar cells using SCAPS, J. Phys. Conf. Ser. 1033 (1) (2018) 012002, https://doi.org/10.1088/1742-6596/1033/1/012002.
[29] Y. Raoui, H. Ez-Zahraouy, N. Tahiri, O. El Bounagui, S. Ahmad, S. Kazim, Performance analysis of $MAPbI_3$ based perovskite solar cells employing diverse charge selective contacts: simulation study, Sol. Energy 193 (2019) 948–955, https://doi.org/10.1016/j.solener.2019.10.009.
[30] S. Gohri, et al., Achieving 24.6% efficiency in 2D perovskite solar cells: bandgap tuning and MXene contact optimization in $(BDA)(MA)n^{-1}PbnI3n^{+1}$ structures, Chem. Phys. Lett. 845 (March) (2024) 141291, https://doi.org/10.1016/j.cplett.2024.141291.
[31] Y. Zheng, et al., Oriented and uniform distribution of Dion–Jacobson phase perovskites controlled by quantum well barrier thickness, Sol. RRL 3 (9) (2019) 1–9, https://doi.org/10.1002/solr.201900090.
[32] Y. Zhang, et al., Effective phase-alignment for 2D halide perovskites incorporating symmetric diammonium ion for photovoltaics, Adv. Sci. 8 (13) (2021) 1–10, https://doi.org/10.1002/advs.202001433.
[33] C. Son, H. Son, B.-S.S. Jeong, Enhanced conversion efficiency in $MAPbI_3$ perovskite solar cells through parameters optimization via SCAPS-1D simulation, Appl. Sci. 14 (6) (2024) 2390, https://doi.org/10.3390/app14062390.
[34] I. Montoya De Los Santos, et al., Optimization of $CH_3NH_3PbI_3$ perovskite solar cells: a theoretical and experimental study, Sol. Energy 199 (ember 2019) (2020) 198–205, https://doi.org/10.1016/j.solener.2020.02.026.
[35] G. Wu, R. Liang, M. Ge, G. Sun, Y. Zhang, G. Xing, Surface passivation using 2D perovskites toward efficient and stable perovskite solar cells, Adv. Mater. 34 (8) (2022) 2105635, https://doi.org/10.1002/adma.202105635.
[36] F. Wang, et al., A multifunctional zinc-based metal-organic framework for sensing and photocatalytic applications, J. Lumin. 194 (2018) 22–28, https://doi.org/10.1016/j.jlumin.2017.10.002.
[37] H. Xue, Z. Chen, S. Tao, G. Brocks, Defects in halide perovskites: does it help to switch from 3D to 2D? ACS Energy Lett. 9 (5) (2024) 2343–2350, https://doi.org/10.1021/acsenergylett.4c00702.
[38] N.L. Adihetty et al., The effect of deep defects on the efficiency variation of $CH_3NH_3PbI_3$ perovskite solar cells, 2021.
[39] M. Mottakin, et al., Design and modelling of eco-friendly $CH_3NH_3SnI_3$-based perovskite solar cells with suitable transport layers, Energies 14 (21) (2021) 7200, https://doi.org/10.3390/en14217200.
[40] A.A. Sutanto, et al., 2D/3D perovskite engineering eliminates interfacial recombination losses in hybrid perovskite solar cells, Chem 7 (7) (2021) 1903–1916, https://doi.org/10.1016/j.chempr.2021.04.002.
[41] C. Ding, et al., Effect of the conduction band offset on interfacial recombination behavior of the planar perovskite solar cells, Nano Energy 53 (9) (2018) 17–26, https://doi.org/10.1016/j.nanoen.2018.08.031.
[42] T. Markvart, L. Castañer, Chapter IA-2 - Semiconductor Materials and Modelling, in: A. McEvoy, L. Castañer, T. Markvart (Eds.), Solar Cells, Second Edition, Elsevier, Amsterdam, The Netherlands, 2013, pp. 27–54.
[43] A. Das, S.D. Peu, M.A.M. Akanda, M.M. Salah, M.S. Hossain, B.K. Das, Numerical simulation and optimization of inorganic lead-free $Cs_3Bi_2I_9$-based perovskite photovoltaic cell: impact of various design parameters, Energies 16 (2023) 2328, https://doi.org/10.3390/en16052328.
[44] Y.M. Lee, et al., Comprehensive understanding and controlling the defect structures: an effective approach for organic-inorganic hybrid perovskite-based solar-cell application, Front. Energy Res. 6 (2018) 1–9, https://doi.org/10.3389/fenrg.2018.00128.
[45] X. Wang, et al., Interfacial modification via a 1,4-butanediamine-based 2D capping layer for perovskite solar cells with enhanced stability and efficiency, ACS Appl. Mater. Interfaces 14 (20) (May 2022) 22879–22888, https://doi.org/10.1021/acsami.1c21036.
[46] P. Chen, Y. Bai, S. Wang, M. Lyu, J.-H. Yun, L. Wang, *In situ* growth of 2D perovskite capping layer for stable and efficient perovskite solar cells, Adv. Funct. Mater. 28 (17) (2018) 1706923, https://doi.org/10.1002/adfm.201706923.
[47] S. Karthick, S. Velumani, J. Bouclé, Experimental and SCAPS simulated formamidinium perovskite solar cells: a comparison of device performance, Sol. Energy 205 (May) (2020) 349–357, https://doi.org/10.1016/j.solener.2020.05.041.
[48] M.S. Islam, et al., Defect study and modelling of SnX3-based perovskite solar cells with SCAPS-1D, Nanomaterials 11 (5) (2021) 1218, https://doi.org/10.3390/nano11051218.
[49] Y. Guo, X. Yin, J. Liu, W. Que, Perspective focusing on mixed-halide Br-rich perovskite solar cells: an inevitable open-circuit voltage deficit derived from photo-induced halide segregation, Matter 5 (7) (2022) 2015–2030, https://doi.org/10.1016/j.matt.2022.05.020.
[50] L.-L. Jiang, et al., Interface engineering toward enhanced efficiency of planar perovskite solar cells, J. Mater. Chem. A 4 (1) (2016) 217–222, https://doi.org/10.1039/C5TA09231K.
[51] T. Ouslimane, L. Et-taya, L. Elmaimouni, A. Benami, Heliyon Impact of absorber layer thickness, defect density, and operating temperature on the performance of $MAPbI_3$ solar cells based on ZnO electron transporting material, Heliyon 7 (February) (2021) e06379, https://doi.org/10.1016/j.heliyon.2021.e06379.
[52] H. Wang, et al., Interlayer cross-linked 2D perovskite solar cell with uniform phase distribution and increased exciton coupling, Sol. RRL 4 (4) (2020) 1–9, https://doi.org/10.1002/solr.201900578.
[53] N.N. Udalova, et al., Butanediammonium salt additives for increasing functional and operando stability of light-harvesting materials in perovskite solar cells, Nanomaterials 12 (24) (2022) 4357, https://doi.org/10.3390/nano12244357.